

3D ANALYSIS AND PREDICTION FOR ASSEMBLY STEP DEVIATIONS OF FOUR-BAR LINKAGE BAY DOORS

Rui Yang, Linkai Yang, Lei Wei & Shiyong Sun

School of Mechanical Engineering, Dalian University of Technology, Dalian 116024

Abstract

To address the lack of effective deviation modeling and analysis methods for complex spatial mechanisms composed of multiple parallel structures, such as four-bar linkage aircraft doors—which renders assembly variations difficult to predict and tolerance design schemes devoid of effective verification—a 3D tolerance analysis method for complex assemblies is proposed, taking into account multiple parallel structures and the kinematic characteristics of the mechanisms. First, based on the small displacement torsor theory, the proposed method equivalently describes the deviations of the parallel structures, thereby simplifying the aircraft door from a complex spatial mechanism into a planar mechanism. Concurrently, considering tolerance principles, mating deviations and geometric feature deviations are equivalently transformed into comprehensive deviations. Taking the step deviation between the fuselage and the follow-up door in the closed state as the functional requirement, the vector loop model of the door is established. Second, a modified forward finite difference method is introduced to improve the calculation efficiency of the Taylor expansion influence coefficients, and singular value decomposition is employed to solve the underdetermined assembly equations. Consequently, the second-order tolerance analysis method is improved to enhance the solving efficiency and generality of the vector loop model. Finally, the proposed method is applied to conduct a 3D tolerance analysis on the four-bar linkage door. The accumulated assembly deviation results of the door are presented, providing a reference basis for evaluating the rationality of the tolerance design scheme.

Keywords: 3D tolerance analysis; second-order tolerance analysis; vector loop model; four-bar linkage door

1. Introduction

The aircraft internal weapon bay door, primarily based on a four-bar linkage mechanism, serves as a crucial component and deployment/retraction mechanism. Due to its effectiveness in fulfilling the stealth requirements of fighter jets, it has emerged as the optimal choice and a developmental trend for payload configurations in advanced fighter aircraft. However, the step and gap between the fuselage skin and movable components such as doors directly compromise the high stealth performance of the aircraft, making rational tolerance design the key to ensuring functional requirements (FRs) like step and gap are met. Assembly deviation analysis of complex assemblies is of paramount importance for achieving rational tolerance design. Currently, the tolerance design of aircraft doors primarily relies on relevant aviation standards and conventional engineering experience, which is implemented by selecting tolerance values or grades for mating features and critical dimensions. This approach fails to evaluate whether the performance requirements can be satisfied from the perspective of the entire assembly. In particular, there is a lack of effective 3D tolerance analysis tools to accurately predict the assembly deviations of the door. Therefore, it is imperative to investigate the 3D accumulation and propagation laws of deviations and to develop applicable 3D tolerance analysis methods. These efforts aim to more accurately predict the assembly deviation range of complex mechanical products and provide critical guidance for product tolerance

https://doi.org/10.71945/icas2026_0140

design.

3D tolerance analysis methods have gradually become the prevailing trend and mainstream in complex product design, primarily including the T-Map model [1], the matrix model [2], the vector loop (VL) model [3], and the Jacobian-torsor (J-T) model [4]. When analyzing the impact of tolerances on critical features, selecting an appropriate tolerance model is of paramount importance [5], the selection should be tailored to the analysis objectives and assembly conditions [6]. In contrast, the VL model constructs implicit assembly functions through vectors, comprehensively representing the geometric structure and tolerance information of the assembly. By holistically constraining the variations of individual deviations from a system-wide perspective, it is more suited for closed-loop system analysis. Furthermore, by introducing small kinematic adjustment, it accurately reflects the deviation propagation characteristics of kinematic mechanisms—a capability lacking in the other models. Therefore, for the 3D tolerance analysis of closed-loop kinematic mechanisms such as the aircraft four-bar linkage door, the VL model demonstrates superior advantages and applicability.

Solution methods for the VL model primarily include the direct linearization method (DLM), the Monte Carlo method (MCM), the second-order tolerance analysis method (SOTA) [7], and the number theory method (NTM) [8]. Among these, the DLM is based on the first-order Taylor expansion of the assembly function, which exhibits lower accuracy in highly nonlinear scenarios. The MCM is better equipped to handle nonlinear problems, but it requires a massive number of samples to obtain accurate results. Compared to the MCM, the NTM can generate more uniformly distributed sets of random points and improves the efficiency of generating these point sets. The SOTA method can achieve an accuracy comparable to that of the MCM without the need to generate random samples. While enhancing the capability of nonlinear tolerance analysis, it substantially improves computational efficiency.

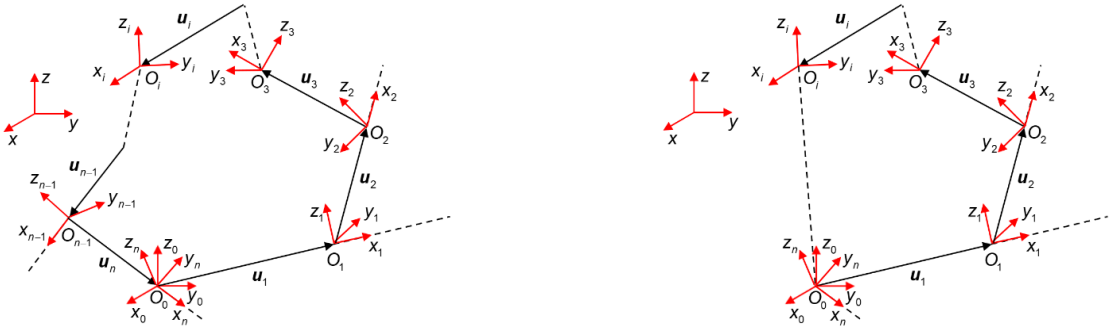
CAO et al. [8] proposed the NTM to solve and analyze the VL model of a crank-slider mechanism. ZHAO et al. [9] incorporated geometric deviations, mating clearances, and assembly deformations into the DLM, providing a novel approach for the assembly precision analysis of complex products. CORRADO et al. [10] employed the VL model to evaluate the nominal position deviation of drilled holes caused by fixture position variations and the shape deviations of contacting parts. KOSEC et al. [11] compared the analysis results of the VL model with those of three other models for open-loop assemblies. Based on the VL model, SCHAECHTL et al. [12] ensured the functionality of non-assembly mechanisms during motion via statistical tolerance analysis that considered geometric deviations and joint clearances. MALTAURO et al. [13] investigated the varying analysis results of applying the SOTA method when non-centered and non-normal actual distributions were used as inputs for simulated assembly analysis. Combining the VL model with skin model shapes, LI et al. [14] realized the geometric precision analysis of the serial structures of aerospace vehicles. Based on the VL model, ZHAO et al. [15] established a rigid-flexible coupled assembly precision analysis method for low-rigidity components. The aforementioned studies demonstrate that the VL model and its solution methods can effectively account for assembly dimensions, geometric tolerances, and mating deviations, while also possessing the capability for kinematic deviation analysis. However, existing studies are either restricted to 2D scenarios or fail to comprehensively consider geometric tolerances, mating clearances, and tolerance principles. Furthermore, there is a lack of deviation description methods tailored for complex assemblies comprising multiple parallel structures [16]. Consequently, these existing methods exhibit certain limitations when applied to the tolerance analysis of four-bar linkage doors.

To investigate the 3D accumulation and propagation laws of deviations in complex assemblies, to develop a rapid and accurate 3D tolerance analysis method for complex mechanical products, and to verify the rationality of the tolerance design for the four-bar linkage door. The aircraft four-bar linkage door is taken as the research object. Combining its kinematic characteristics, assembly features, and tolerance principles, a simplified description of the deviations in multiple parallel structures is formulated based on the small displacement torsor (SDT) theory. Subsequently, taking

the step deviation between the fuselage and the follow-up door in the closed state as the FR, a 3D VL model is established. Furthermore, to fulfill the computational demands of the model and enhance the applicability and efficiency of the solving process, a solution method for underdetermined assembly constraint equations and the modified forward finite difference (ModFFD) method are incorporated into the SOTA method. This integration yields a more stable and efficient improved SOTA method. Finally, based on the proposed simplified 3D tolerance modeling method for complex parallel spatial mechanisms and the improved SOTA method, a 3D tolerance analysis procedure for the aircraft four-bar linkage door is established, successfully realizing the prediction of its accumulated assembly deviations.

2. Establishment of the 3D vector loop model for the four-bar linkage door

2.1 Overview of the 3D vector loop model



(a) Closed vector loop. (b) Open vector loop.

Figure 1 – Schematic diagram of the 3D vector loop.

In the VL model, deviations in mechanical assemblies are classified into the following three categories: (1) dimensional deviation: represented by a vector whose magnitude is the nominal dimension or angle, accompanied by a specified deviation range; (2) geometric feature deviation: represented by a vector with a magnitude of zero, accompanied by a specified deviation range; (3) assembly adjustment deviation: represented by a vector whose magnitude is a nominal value, accompanied by an unknown deviation range. The first two categories of deviations are generated during the manufacturing process. They are classified as manufacturing variables, remain unaffected by other variables, and correspond to the constituent links in tolerance analysis. The third category of deviation is determined by the degrees of freedom of the kinematic joints formed at the mating features of the assembly, with the type of kinematic joint dictated by the mating type and mating conditions. This deviation is influenced by the first two categories and is classified as an assembly variable. The core philosophy of the VL model is to express these three categories of deviations in the form of vectors and connect them into a vector loop in accordance with the assembly method and sequence, thereby accomplishing the tolerance modeling of the assembly. The FR serves as the objective of the tolerance analysis, namely the closing link, which also falls within the scope of assembly variables.

Figure 1 illustrates the schematic of the 3D VL model. Figure 1a displays a closed vector loop, which is utilized to position the individual components and kinematic joints within the assembly, defining the kinematic closure constraints of the assembly. Figure 1b depicts an open vector loop, which is employed to describe a certain clearance or the accumulated tolerance result within the assembly, reflecting its FR. For both closed and open loops, the implicit assembly functions are formulated through the multiplication of homogeneous transformation matrix (HTM).

Due to the influence of geometric tolerances or assembly deviations, the pose of the local coordinate system undergoes translational or rotational variations. Consequently, the degrees of freedom and the ranges of these variations must be determined based on the geometric features, mating types, and specific tolerance items. These variations are then mathematically represented by HTM and

integrated into the vector loop in an appropriate sequence to formulate the final assembly equations, as expressed in Eqs. (1) and (2). Specifically, Eq. (1) represents the closed-loop vector equation, while Eq. (2) denotes the open-loop vector equation.

$$\boldsymbol{R}_1 \cdot \boldsymbol{T}_1 \cdot \boldsymbol{R}_2 \cdot \boldsymbol{T}_2 \cdots \boldsymbol{R}_i \cdot \boldsymbol{T}_i \cdot \boldsymbol{T}_{it} \cdot \boldsymbol{R}_{it} \cdots \boldsymbol{R}_n \cdot \boldsymbol{T}_n \cdot \boldsymbol{R}_e = \boldsymbol{I} \tag{1}$$

$$\boldsymbol{G} = \boldsymbol{R}_1 \cdot \boldsymbol{T}_1 \cdot \boldsymbol{R}_2 \cdot \boldsymbol{T}_2 \cdots \boldsymbol{R}_i \cdot \boldsymbol{T}_i \cdot \boldsymbol{T}_{it} \cdot \boldsymbol{R}_{it} \cdot \boldsymbol{R}_e \tag{2}$$

Where $\boldsymbol{R}_i$ and $\boldsymbol{T}_i$ represent the rotation matrix and translation matrix of the *i*-th local coordinate system, respectively; $\boldsymbol{R}_{it}$ and $\boldsymbol{T}_{it}$ are the products of the rotation matrices and translation matrices, respectively, constituted by geometric feature deviations, mating deviations, or small kinematic adjustments at the *i*-th local coordinate system; $\boldsymbol{R}_e$ is the final rotation matrix that aligns the orientation of the end coordinate system of the vector loop with that of the initial coordinate system; $\boldsymbol{I}$ is the identity matrix; and $\boldsymbol{G}$ is the result matrix of the open-loop assembly function.

2.2 Analysis and simplification of the four-bar linkage door mechanism

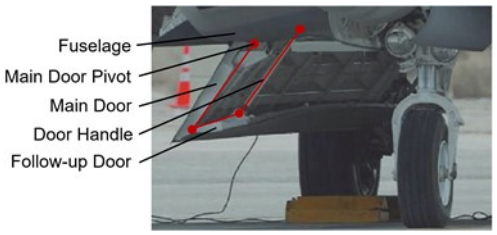


Figure 2 – The F-22 internal weapon bay door.

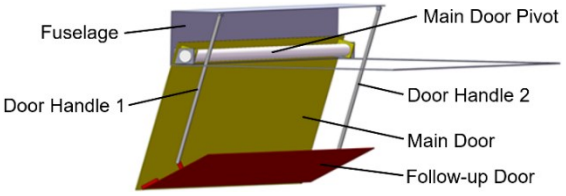


Figure 3 – Schematic diagram of the bay door in the open position.

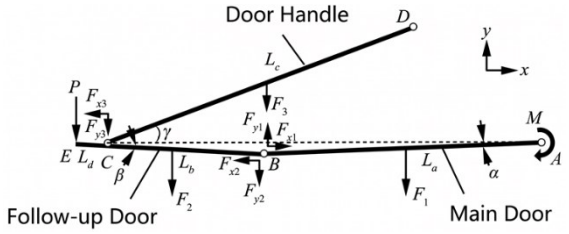


Figure 4 – Structural schematic of the internal weapon bay door.

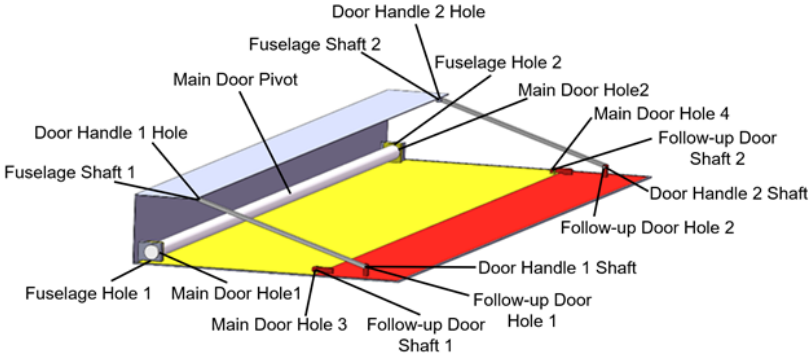


Figure 5 – Simplified model of the door.

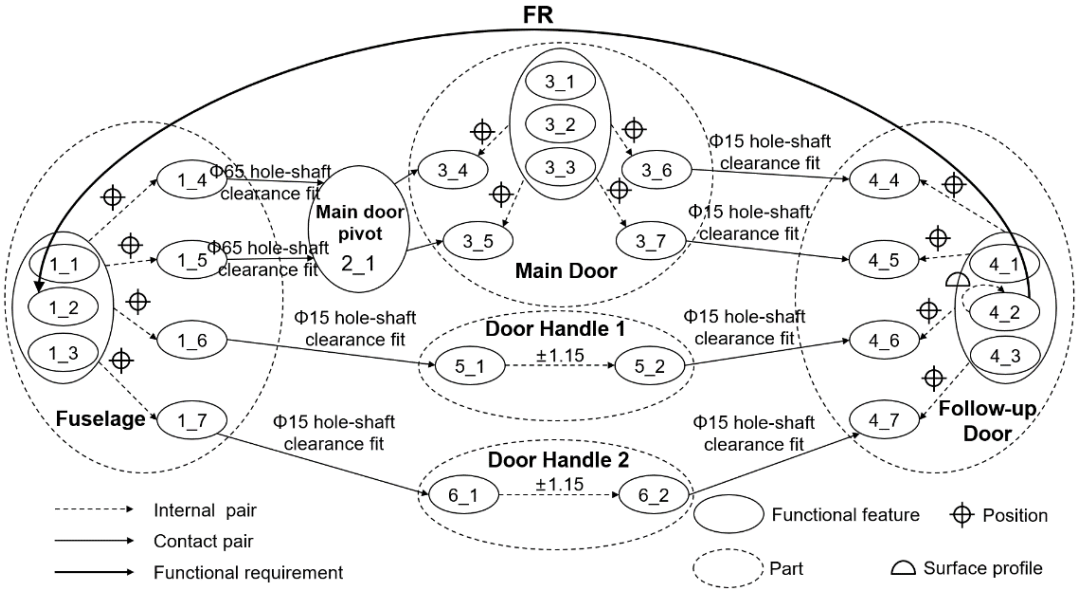
Figure 2 shows the four-bar linkage internal weapon bay door of the U.S. F-22 aircraft. The bay is located directly beneath the fuselage, and the door system consists of a pair of outward-opening folding mechanisms. Each side adopts a four-bar linkage mechanism design composed of a main door, a follow-up door, door handles, and the fuselage structure. Figure 4 presents the structural schematic of the door. The opening and closing of the door are driven by a rotary actuator. The fixed lug of the actuator is connected to the fuselage structure, while the movable lug is connected to the main door and is positioned on the main door pivot. One side of the follow-up door is connected to

the main door via hinges, and the other side is connected to two door handles. The actuator drives the main door pivot, causing the main door to execute a rotational motion, which consequently drives the follow-up door and the door handles to realize the overall opening and closing actuation.

Table 1 – Key dimensions and tolerance information of the door components.

Dimension / tolerance item	Nominal (mm)	Tolerance (mm)	Principle	Datums
Fuselage hole 1 / 2 position	0	0.5	MMR	Fuselage left, bottom, and rear surfaces
Fuselage hole 1 / 2 diameter	65	[0,+0.3]	—	—
Main door pivot diameter	65	[-0.3,0]	—	—
Main door hole 1 / 2 position	0	0.5	MMR	Main door left, bottom, and rear surfaces
Main door hole 1 / 2 diameter	65	—	—	—
Main door hole 3 / 4 position	0	0.5	MMR	Main door left, bottom, and rear surfaces
Main door hole 3 / 4 diameter	15	[0,+0.18]	—	—
Follow-up door shaft 1 / 2 position	0	0.5	MMR	Follow-up door left, bottom, and rear surfaces
Follow-up door shaft 1 / 2 diameter	15	[-0.18,0]	—	—
Follow-up door hole 1 / 2 position	0	0.5	MMR	Follow-up door left, bottom, and rear surfaces
Follow-up door hole 1 / 2 diameter	15	[0,+0.18]	—	—
Door handle 1 / 2 shaft diameter	15	[-0.18,0]	—	—
Door handle 1 / 2 hole diameter	15	[0,+0.18]	—	—
Door handle 1 / 2 center distance	801.087	[-1.15,+1.15]	—	—
Fuselage shaft 1 / 2 position	0	0.5	MMR	Fuselage left, bottom, and rear surfaces
Fuselage shaft 1 / 2 diameter	15	[-0.18,0]	—	—
Follow-up door bottom surface profile	0	0.6	—	—
Fuselage hole 1 – 2 span	3810	—	—	—
Main door hole 1 – 2 span	3750	—	—	—
Main door hole 3 – 4 span	3710	—	—	—
Follow-up door hole 1 – 2 span	3750	—	—	—
door handle 1 – 2 hole span	3790	—	—	—

In the closed state, the step between the follow-up door and the fuselage bottom surface directly affects the Radar Cross Section (RCS) of the aircraft. A larger RCS value increases the probability of radar detection, necessitating strict control over this dimension. Consequently, the vertical step between the follow-up door and the fuselage bottom is defined as the FR of the system. The poses of the components are primarily determined by the following assembly constraints: the hole-shaft fit between the main door holes and the pivot, the hinge connections between the main door and the follow-up door, the hinge connections between the follow-up door and the two door handles, and the hinge connections between the door handles and the fuselage. Based on the structural layout and fit types, the door mechanism is simplified for analysis (as shown in Figure 5). Referring to HB 5800-2021 and other relevant standards, Table 1 lists the key dimensions and tolerance information for each component in the model. Based on the aforementioned assembly relationships, the assembly connection diagram of the door is established, as illustrated in Figure 6.



1_1, 1_2, 1_3 – Left, bottom and rear surfaces of the fuselage; 1_4, 1_5 – Fuselage holes 1 and 2; 1_6, 1_7 – Fuselage shafts 1 and 2; 2_1 – Main door pivot; 3_1, 3_2, 3_3 – Left, bottom, rear surfaces of the main door; 3_4, 3_5 – Main door holes 1 and 2; 3_6, 3_7 – Main door holes 3 and 4; 4_1, 4_2, 4_3 – Left, bottom, rear surfaces of the follow-up door; 4_4, 4_5 – Follow-up door shafts 1 and 2; 4_6, 4_7 – Follow-up door holes 1 and 2; 5_1, 5_2 – door handle 1 hole and shaft;6_1, 6_2 – door handle 2 hole and shaft;

Figure 6 – Assembly connection diagram of the door mechanism.

2.3 Deviation equivalency of the door parallel structure

A parallel structure refers to a configuration where the spatial pose of a specific component is simultaneously constrained by multiple kinematic branches, a common occurrence in revolute mechanisms. The door system contains numerous such structures, such as the fits between the fuselage and pivot, the main door and the follow-up door, and the follow-up door and the door handles. While VL models are widely employed for spatial serial dimensional chains, applying them to parallel structures by analyzing only a single branch leads to an approximation that loses significant tolerance information. Such a simplification often fails to align with the actual assembly state. Consequently, it is essential to implement specialized treatments for parallel deviation propagation to enhance the precision and reliability of the analysis results.

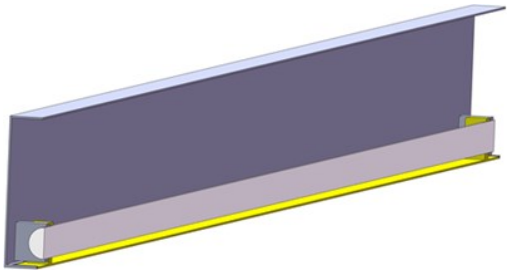


Figure 7 – Parallel structure among the fuselage, main door, and main door pivot.

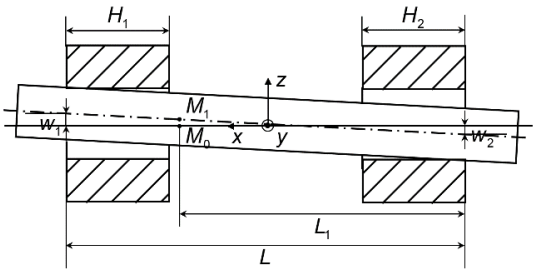


Figure 8 – Schematic diagram of the parallel structure.

Figure 8 illustrates the schematic diagram of the parallel structure. The left and right holes collectively constrain the spatial pose of the shaft. Specifically, the shaft forms connection pair FE_1 with the left hole and connection pair FE_2 with the right hole. When analyzing them independently, according to the SDT theory, the deviations of the two connection pairs in the coordinate system of Figure 8 are

expressed as follows:

$$\boldsymbol{s}_{FE_1} = \begin{bmatrix} 0 & v_1 & w_1 & 0 & \beta_1 & \gamma_1 \end{bmatrix}^T \tag{3}$$

$$\boldsymbol{s}_{FE_2} = \begin{bmatrix} 0 & v_2 & w_2 & 0 & \beta_2 & \gamma_2 \end{bmatrix}^T \tag{4}$$

In the equation, w_1 and w_2 represent the variations of the actual axis relative to the ideal axis in the z-direction at FE_1 and FE_2, respectively. To represent the pose deviation of the actual shaft, an arbitrary point M_0 is selected on the ideal axis, and the SDT at this point is used to characterize the overall variation of the shaft. As illustrated in Figure 8, the overall displacement of the shaft is determined by w_1, w_2, L_1, and L. Based on the geometric relationships, the distance from M_0 to M_1 in the z-direction is derived as:

$$w_M = \frac{L_1 (w_1 - w_2)}{L} + w_2 \tag{5}$$

The rotational variation from M_0 to M_1 is derived as:

$$\beta_M = \arctan\left(\frac{w_2 - w_1}{L} \right) \tag{6}$$

Since β_M is a small variation, it can be approximated as $\beta_M \approx (w_2 - w_1) / L$. Similarly, the variations from M_0 to M_1 in the xoy plane are obtained using the same method. Finally, the SDT at point M_0 is expressed as:

$$\boldsymbol{s}_{M_0} = \begin{bmatrix} 0 & \dfrac{L_1 (v_1 - v_2)}{L} + v_2 & \dfrac{L_1 (w_1 - w_2)}{L} + w_2 & 0 & \dfrac{w_2 - w_1}{L} & \dfrac{v_1 - v_2}{L} \end{bmatrix}^T \tag{7}$$

By calculating the pose variation of the parallel structure based on Eq. (7) and representing it with a deviation HTM, it can be integrated into the assembly equation. Thus, the VL model incorporating parallel structures is established.

2.4 Description of hole-shaft fit deviations considering Maximum Material Requirement

Tolerance principles are the fundamental rules governing the relationship between dimensional tolerances and geometric tolerances. In the design and manufacturing of mechanical products, the appropriate application of these principles not only simplifies the fabrication, inspection, and assembly processes—thereby reducing costs and enhancing product quality—but also improves component interchangeability and economic efficiency [17]. Consequently, to guarantee that the hole-shaft fits within the door mechanism satisfy assembly conditions and kinematic requirements under varying states—preventing jamming during opening or closing operations— the maximum material requirement (MMR) is applied to the critical fits of the system.



(a) Shaft with specified MMR. (b) Hole with specified MMR.

Figure 9 – Hole and shaft features with specified MMR.

Figure 9 illustrates the hole and shaft features with specified MMR. The nominal diameters of the shaft and hole are denoted by d and D, respectively. The upper and lower deviations for the shaft are defined as Δd_U and Δd_L, while those for the hole are ΔD_U and ΔD_L. The positional tolerances of the shaft and hole relative to datum A are specified as t_p and T_p, respectively.

Under the positional tolerance constraint with MMR, the Maximum Material Virtual Size (MMVS) of the shaft is $d_{MV} = d + \Delta d_U + t_p$, and its Least Material Virtual Size (LMVS) is $d_{LV} = d + 2\Delta d_L - t_p - \Delta d_U$. Similarly, the MMVS of the hole is $D_{MV} = D + \Delta D_L - T_p$, and its LMVS is $D_{LV} = D + 2\Delta D_U + T_p - \Delta D_L$. Consequently, the minimum clearance of the hole-shaft fit is derived as:

$$C_{\min} = D_{MV} - d_{MV} = D - d + \Delta D_L - \Delta d_U - T_p - t_p \tag{8}$$

the maximum clearance of the hole-shaft fit is derived as:

$$C_{\max} = D_{LV} - d_{LV} = D - d + 2\Delta D_U - 2\Delta d_L + T_p + t_p - \Delta D_L + \Delta d_U \tag{9}$$

Based on Eqs. (8) and (9), the clearance range for the hole-shaft fit under MMR can be determined. Let C denote the actual assembly clearance. If $C_{\min} \leq 0$, then $C \in [0, C_{\max}]$; if $C_{\min} > 0$, then $C \in [C_{\min}, C_{\max}]$. To facilitate subsequent calculations, this clearance range is expressed using the SDT theory. Assuming the x-axis of the local coordinate system aligns with the shaft axis and the engagement length of the fit is l, then for the case where $C_{\min} \leq 0$:

$$\boldsymbol{s}_C = \left[0 \quad \left[-\frac{C_{\max}}{2}, \frac{C_{\max}}{2} \right] \quad \left[-\frac{C_{\max}}{2}, \frac{C_{\max}}{2} \right] \quad 0 \quad \left[-\frac{C_{\max}}{l}, \frac{C_{\max}}{l} \right] \quad \left[-\frac{C_{\max}}{l}, \frac{C_{\max}}{l} \right] \right]^T \tag{10}$$

When $C_{\min} > 0$:

$$\boldsymbol{s}_C = \left[\begin{array}{c} 0 \\ \left[-\frac{C_{\max} - C_{\min}}{2}, \frac{C_{\max} - C_{\min}}{2} \right] \\ \left[-\frac{C_{\max} - C_{\min}}{2}, \frac{C_{\max} - C_{\min}}{2} \right] \\ 0 \\ \left[-\frac{C_{\max} - C_{\min}}{l}, \frac{C_{\max} - C_{\min}}{l} \right] \\ \left[-\frac{C_{\max} - C_{\min}}{l}, \frac{C_{\max} - C_{\min}}{l} \right] \end{array} \right] \tag{11}$$

2.5 Construction of the door vector loop model

Based on the simplified door mechanism illustrated in Figure 5, a 3D VL model is formulated. The FR of the system is defined as the vertical step between the follow-up door and the bottom surface of the fuselage. Geometrically, this step is evaluated by the vertical distance between the center point of the follow-up door and its corresponding projection point on the fuselage bottom surface. The formulation process is detailed as follows:

Based on the theories established in Sections 2.3 and 2.4, the deviations of the parallel structure are equivalently represented at the center point of the structure, thereby simplifying the complex spatial mechanism into an equivalent planar mechanism. Taking the hole-shaft fit between the fuselage and the main door pivot as a case study: According to Table 1, both fuselage hole 1 and hole 2 are subject to a positional tolerance of 0.5 mm under the MMR. The nominal diameter of the holes is 65 mm, with a dimensional tolerance of [0, +0.3] mm. Consequently, the MMVS and LMVS of the two holes are calculated as 64.5 mm and 66.1 mm, respectively. Similarly, the main door pivot has a nominal

diameter of 65 mm with a dimensional tolerance of [-0.3, 0] mm. Its MMVS and LMVS are determined to be 65 mm and 64.7 mm, respectively.

Based on Eqs. (8) and (9), the maximum and minimum clearances of this fit are calculated as 1.4 mm and -0.5 mm, respectively. Substituting these values into Eq. (10), and assuming the *x*-axis of the local coordinate system aligns with the main door pivot axis, the deviations $\boldsymbol{s}_{1l}$ and $\boldsymbol{s}_{1r}$ of the pivot axis at fuselage hole 1 and fuselage hole 2 can be obtained:

$$\boldsymbol{s}_{1l} = \boldsymbol{s}_{1r} = \left[0 \quad \left[-\frac{1.4}{2}, \frac{1.4}{2}\right] \quad \left[-\frac{1.4}{2}, \frac{1.4}{2}\right] \quad 0 \quad \left[-\frac{1.4}{l_1}, \frac{1.4}{l_1}\right] \quad \left[-\frac{1.4}{l_1}, \frac{1.4}{l_1}\right]\right]^T \tag{12}$$

In the equation, l_1 denotes the engagement length of the main door pivot with fuselage hole 1 and fuselage hole 2, respectively. Given the total span of 3810 mm between the two holes, the pose variation of the pivot, evaluated at its midpoint M_0 according to Eq. (7), can be expressed as:

$$\boldsymbol{s}_1 = \left[0 \quad \frac{\boldsymbol{s}_{1l}^y + \boldsymbol{s}_{1r}^y}{2} \quad \frac{\boldsymbol{s}_{1l}^z + \boldsymbol{s}_{1r}^z}{2} \quad 0 \quad \frac{\boldsymbol{s}_{1l}^z - \boldsymbol{s}_{1r}^z}{3810} \quad \frac{\boldsymbol{s}_{1r}^y - \boldsymbol{s}_{1l}^y}{3810}\right]^T \tag{13}$$

Where $\boldsymbol{s}_{1l}^y$ and $\boldsymbol{s}_{1l}^z$ represent the translation components of the deviation $\boldsymbol{s}_{1l}$ (between the main door pivot and fuselage hole 1) along the *y*- and *z*-axes of the local coordinate system, respectively. Similarly, $\boldsymbol{s}_{1r}^y$ and $\boldsymbol{s}_{1r}^z$ denote the translation components of the deviation $\boldsymbol{s}_{1r}$ (associated with fuselage hole 2) along the respective *y*- and *z*-axes. The rotational components of the integrated deviation $\boldsymbol{s}_1$ depend on the spatial orientation of the local coordinate system. By the same token, the deviations of the remaining four parallel hole-shaft fits are equivalently mapped and described at their respective center points. Table 2 presents the analytical deviation expressions for each branch of the five parallel structures.

Table 2 – Deviations of individual branches in the parallel structures.

Variables	Description	Representation of variation range
$\boldsymbol{s}_{1l}$, $\boldsymbol{s}_{1r}$	Main door pivot and fuselage hole 1 / 2 branch deviations	$\left[\pm\frac{1.4}{2}, \pm\frac{1.4}{2}, 0, \pm\frac{1.4}{l_1}, \pm\frac{1.4}{l_1}, 0\right]^T$
$\boldsymbol{s}_{2l}$, $\boldsymbol{s}_{2r}$	Main door pivot and main door hole 1 / 2 branch deviations	$\left[\pm\frac{0.5}{2}, \pm\frac{0.5}{2}, 0, \pm\frac{0.5}{l_2}, \pm\frac{0.5}{l_2}, 0\right]^T$
$\boldsymbol{s}_{3l}$, $\boldsymbol{s}_{3r}$	Main door hole 3 / 4 and follow-up door shaft 1 / 2 branch deviations	$\left[\pm\frac{1.72}{2}, \pm\frac{1.72}{2}, 0, \pm\frac{1.72}{l_3}, \pm\frac{1.72}{l_3}, 0\right]^T$
$\boldsymbol{s}_{4l}$, $\boldsymbol{s}_{4r}$	Follow-up door hole 1 / 2 and door handle 1 / 2 shaft branch deviations	$\left[\pm\frac{1.04}{2}, \pm\frac{1.04}{2}, 0, \pm\frac{1.04}{l_4}, \pm\frac{1.04}{l_4}, 0\right]^T$
$\boldsymbol{s}_{5l}$, $\boldsymbol{s}_{5r}$	Door handle 1 / 2 hole and fuselage shaft 1 / 2 branch deviations	$\left[\pm\frac{1.04}{2}, \pm\frac{1.04}{2}, 0, \pm\frac{1.04}{l_5}, \pm\frac{1.04}{l_5}, 0\right]^T$

Building upon this foundation, a global coordinate system, denoted as $x_0y_0z_0$, is established with its origin defined at a specific point on the centerline of the fuselage's bottom surface. Taking into account the assembly relationships of the door components (as depicted in Figure 6), alongside the geometric locations of the datum and mating features, local coordinate systems are systematically assigned. Initially, the hole-shaft fit between the fuselage and the pivot is located using the nominal locating dimensions *A* and *B*. Subsequently, nominal dimensions *C*, *D*, and *E* are utilized to determine the joint position between the main door and the follow-up door. By incorporating the structural features of the follow-up door and locating dimensions *F*, *G*, *H*, and *I*, the joint between the door

handle and the follow-up door is identified. The kinematic chain then extends along the nominal length *J* of the door handle to its connection point with the fuselage. Finally, the nominal dimensions *K*, *L*, and *M* of the fuselage trace the path back to the global origin. This continuous sequence explicitly defines the deviation transmission path and constitutes the closed vector loop of the door mechanism, as illustrated in Figures. 10 and 11.

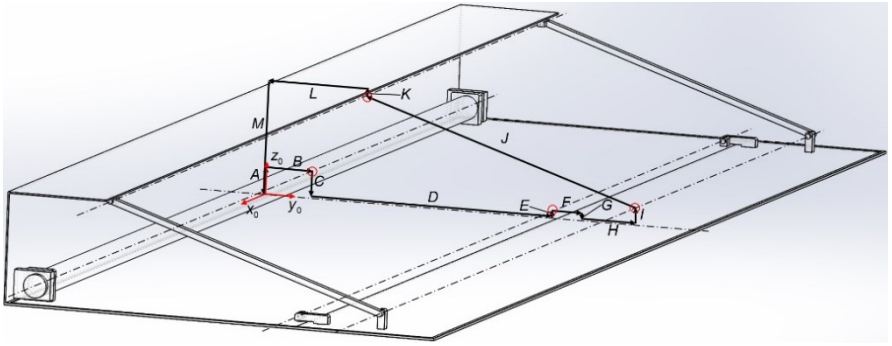


Figure 10 – Deviation transmission path of the bay door.

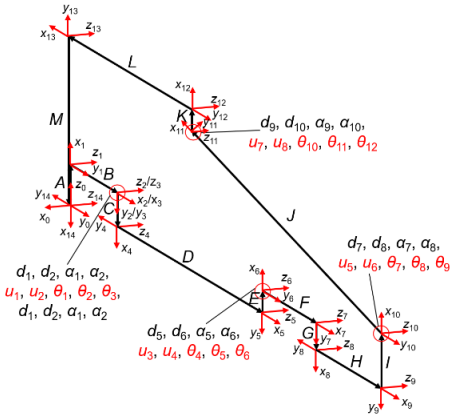


Figure 11 – Closed vector loop representation of bay door deviations.

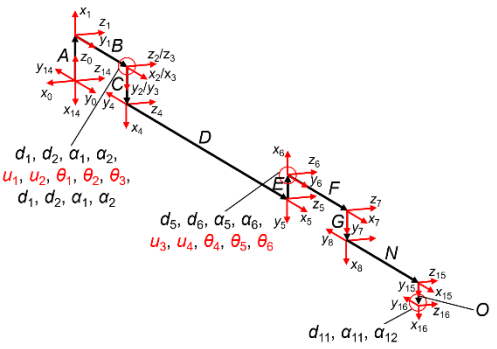


Figure 12 – Open vector loop representation of bay door deviations.

Once the deviation transmission path is established, it is necessary to consider geometric tolerances, joint clearances, and kinematic assembly adjustments by introducing specific variables to formulate the deviation HTM. Taking the fit between the main door pivot and the fuselage holes as an example, the deviations are equivalently mapped to the local coordinate system $x_2y_2z_2$ located at the center of the pivot axis. At this point, four manufacturing deviation variables are present: the translational deviations d_1 and d_2 of the actual pivot center relative to the ideal center along the x_2 and y_2 directions, and the rotational deviations α_1 and α_2 about the x_2 and y_2 axes. Concurrently, during the final assembly adjustment process, five assembly adjustment variables are introduced at this joint: the translational adjustments u_1 and u_2 along the x_2 and y_2 directions; the rotational adjustments θ_1 and θ_2 about the x_2 and y_2 axes; and the rotational adjustment θ_3 about its own longitudinal axis, the z_2-axis.

As the main door pivot directly drives the rotation of the main door, an interference fit or other rigid connection is typically adopted between them. Consequently, the pose of the main door is entirely determined by the pivot, eliminating the need to consider any joint clearance deviations between these two components. However, because the holes on both sides of the main door possess a positional tolerance subject to the MMR relative to the door's datum, a relative pose deviation between the main door and the pivot inevitably occurs. Applying the equivalence mapping principle, the positional deviations from both sides are equivalently mapped and characterized at the center coordinate system of the main door hole axis, $x_3y_3z_3$. The pose of this coordinate system aligns

identically with that of $x_2y_2z_2$ after accounting for all preceding deviations and kinematic adjustments. At this juncture, four manufacturing deviation variables are introduced: the translational deviations d_3 and d_4 of the hole axis center along the x_3 and y_3 axes, and the rotational deviations α_3 and α_4 about the x_3 and y_3 axes. The variables for the remaining three parallel hole-shaft fits in the system are introduced following the exact same logical framework as the fit between the main door pivot and the fuselage.

Table 3 – Detailed information of the variables.

Variables	Description	Nominal (mm)	range / expression	type
A	fuselage dimension	50	0	manufacturing
B	fuselage dimension	65	0	manufacturing
C	main door dimension	46	0	manufacturing
D	main door dimension	720	0	manufacturing
E	main door dimension	15	0	manufacturing
F	follow-up door dimension	85	0	manufacturing
G	follow-up door dimension	15	0	manufacturing
H	follow-up door dimension	140	0	manufacturing
I	follow-up door dimension	45	0	manufacturing
J	door handle dimension	801.087	[-1.15, +1.15]	manufacturing
K	fuselage dimension	10	0	manufacturing
L	fuselage dimension	240	0	manufacturing
M	fuselage dimension	280	0	manufacturing
N	follow-up door dimension	120	0	manufacturing
O	follow-up door dimension	4	0	manufacturing
d_1, d_2	translational deviation at fuselage / pivot fit (x_2, y_2)	0	$d_1 = \frac{s_{1l}^x + s_{1r}^x}{2}, d_2 = \frac{s_{1l}^y + s_{1r}^y}{2}$	manufacturing
α_1, α_2	rotational deviation at fuselage / pivot fit (x_2, y_2)	0	$\alpha_1 = \frac{s_{1l}^y - s_{1r}^y}{3810}, \alpha_2 = \frac{s_{1r}^x - s_{1l}^x}{3810}$	manufacturing
u_1, u_2	translational adjustment at fuselage / pivot fit (x_2, y_2)	0	Unknown	assembly
θ_1, θ_2, θ_3	rotational adjustment at fuselage / pivot fit (x_2, y_2, z_2) and the main door pivot	0	Unknown	assembly
d_3, d_4	main door hole 1 / 2 position deviation (x_3, y_3)	0	$d_3 = \frac{s_{2l}^x + s_{2r}^x}{2}, d_4 = \frac{s_{2l}^y + s_{2r}^y}{2}$	manufacturing
α_3, α_4	main door hole 1 / 2 position deviation (x_3, y_3)	0	$\alpha_3 = \frac{s_{2l}^y - s_{2r}^y}{3750}, \alpha_4 = \frac{s_{2r}^x - s_{2l}^x}{3750}$	manufacturing
d_5, d_6	translational deviation at main / follow-up door fit (x_6, y_6)	0	$d_5 = \frac{s_{3l}^x + s_{3r}^x}{2}, d_6 = \frac{s_{3l}^y + s_{3r}^y}{2}$	manufacturing
α_5, α_6	rotational deviation at main / follow-up door fit (x_6, y_6)	0	$\alpha_5 = \frac{s_{3l}^y - s_{3r}^y}{3710}, \alpha_6 = \frac{s_{3r}^x - s_{3l}^x}{3710}$	manufacturing
u_3, u_4	translational adjustment at main / follow-up door fit (x_6, y_6)	0	Unknown	assembly
θ_4, θ_5, θ_6	rotational adjustment at main / follow-up door fit (x_6, y_6, z_6)	0	Unknown	assembly
d_7, d_8	translational deviation at follow-up door / handle fit (x_{10}, y_{10})	0	$d_7 = \frac{s_{4l}^x + s_{4r}^x}{2}, d_8 = \frac{s_{4l}^y + s_{4r}^y}{2}$	manufacturing
α_7, α_8	rotational deviation at follow-up door / handle fit (x_{10}, y_{10})	0	$\alpha_7 = \frac{s_{4l}^y - s_{4r}^y}{3750}, \alpha_8 = \frac{s_{4r}^x - s_{4l}^x}{3750}$	manufacturing

u_5, u_6	translational adjustment at follow-up door / handle fit (x_{10}, y_{10})	0	Unknown	assembly
θ_7, θ_8	rotational adjustment at follow-up door / handle fit (x_{10}, y_{10})	0	Unknown	assembly
θ_9	rotational adjustment at follow-up door / handle fit (z_{10})	-73.985°	Unknown	assembly
d_9, d_{10}	translational deviation at handle / fuselage fit (x_{11}, y_{11})	0	$d_9 = \frac{s_{5l}^x + s_{5r}^x}{2}, d_{10} = \frac{s_{5l}^y + s_{5r}^y}{2}$	manufacturing
α_9, α_{10}	rotational deviation at handle / fuselage fit (x_{11}, y_{11})	0	$\alpha_9 = \frac{s_{5l}^y - s_{5r}^y}{3790}, \alpha_{10} = \frac{s_{5r}^x - s_{5l}^x}{3790}$	manufacturing
u_7, u_8	translational adjustment at handle / fuselage fit (x_{11}, y_{11})	0	Unknown	assembly
θ_{10}, θ_{11}	rotational adjustment at handle / fuselage fit (x_{11}, y_{11})	0	Unknown	assembly
θ_{12}	rotational adjustment at handle / fuselage fit (z_{11})	73.985°	Unknown	assembly
d_{11}	follow-up door bottom surface profile deviation (x_{16})	0	[-0.3, +0.3]	manufacturing
α_{11}	follow-up door bottom surface profile deviation (y_{16})	0	$\left[-\frac{0.6}{3930}, +\frac{0.6}{3930}\right]$	manufacturing
α_{12}	follow-up door bottom surface profile deviation (z_{16})	0	$\left[-\frac{0.6}{385}, +\frac{0.6}{385}\right]$	manufacturing

$$\begin{aligned}
&\boldsymbol{R}_y(-\pi/2)\boldsymbol{T}_x(A)\boldsymbol{R}_z(\pi/2)\boldsymbol{T}_x(B)\boldsymbol{T}_x(d_1)\boldsymbol{T}_y(d_2)\boldsymbol{R}_x(\alpha_1)\boldsymbol{R}_y(\alpha_2)\boldsymbol{T}_x(u_1)\boldsymbol{T}_y(u_2)\boldsymbol{R}_x(\theta_1)\boldsymbol{R}_y(\theta_2)\\
&\boldsymbol{R}_z(\theta_3)\boldsymbol{T}_x(d_3)\boldsymbol{T}_y(d_4)\boldsymbol{R}_x(\alpha_3)\boldsymbol{R}_y(\alpha_4)\boldsymbol{R}_z(\pi/2)\boldsymbol{T}_x(C)\boldsymbol{R}_z(-\pi/2)\boldsymbol{T}_x(D)\boldsymbol{R}_z(-\pi/2)\boldsymbol{T}_x(E)\\
&\boldsymbol{T}_x(d_5)\boldsymbol{T}_y(d_6)\boldsymbol{R}_x(\alpha_5)\boldsymbol{R}_y(\alpha_6)\boldsymbol{T}_x(u_3)\boldsymbol{T}_y(u_4)\boldsymbol{R}_x(\theta_4)\boldsymbol{R}_y(\theta_5)\boldsymbol{R}_z(\theta_6)\boldsymbol{R}_z(\pi/2)\boldsymbol{T}_x(F)\boldsymbol{R}_z(\pi/2)\\
&\boldsymbol{T}_x(G)\boldsymbol{R}_z(-\pi/2)\boldsymbol{T}_x(H)\boldsymbol{R}_z(-\pi/2)\boldsymbol{T}_x(I)\boldsymbol{T}_x(d_7)\boldsymbol{T}_y(d_8)\boldsymbol{R}_x(\alpha_7)\boldsymbol{R}_y(\alpha_8)\boldsymbol{T}_x(u_5)\boldsymbol{T}_y(u_6)\boldsymbol{R}_x(\theta_7)\\
&\boldsymbol{R}_y(\theta_8)\boldsymbol{R}_z(\theta_9)\boldsymbol{T}_x(J)\boldsymbol{T}_x(d_9)\boldsymbol{T}_y(d_{10})\boldsymbol{R}_x(\alpha_9)\boldsymbol{R}_y(\alpha_{10})\boldsymbol{T}_x(u_7)\boldsymbol{T}_y(u_8)\boldsymbol{R}_x(\theta_{10})\boldsymbol{R}_y(\theta_{11})\boldsymbol{R}_z(\theta_{12})\\
&\boldsymbol{T}_x(K)\boldsymbol{R}_z(-\pi/2)\boldsymbol{T}_x(L)\boldsymbol{R}_z(-\pi/2)\boldsymbol{T}_x(M)\boldsymbol{R}_y(\pi/2)\boldsymbol{R}_x(\pi) = \boldsymbol{I}_{4\times4}
\end{aligned} \tag{14}$$

$$\begin{aligned}
\boldsymbol{G} = {}& \boldsymbol{R}_y(-\pi/2)\boldsymbol{T}_x(A)\boldsymbol{R}_z(\pi/2)\boldsymbol{T}_x(B)\boldsymbol{T}_x(d_1)\boldsymbol{T}_y(d_2)\boldsymbol{R}_x(\alpha_1)\boldsymbol{R}_y(\alpha_2)\boldsymbol{T}_x(u_1)\boldsymbol{T}_y(u_2)\boldsymbol{R}_x(\theta_1)\boldsymbol{R}_y(\theta_2)\\
&\boldsymbol{R}_z(\theta_3)\boldsymbol{T}_x(d_3)\boldsymbol{T}_y(d_4)\boldsymbol{R}_x(\alpha_3)\boldsymbol{R}_y(\alpha_4)\boldsymbol{R}_z(\pi/2)\boldsymbol{T}_x(C)\boldsymbol{R}_z(-\pi/2)\boldsymbol{T}_x(D)\boldsymbol{R}_z(-\pi/2)\boldsymbol{T}_x(E)\boldsymbol{T}_x(d_5)\\
&\boldsymbol{T}_y(d_6)\boldsymbol{R}_x(\alpha_5)\boldsymbol{R}_y(\alpha_6)\boldsymbol{T}_x(u_3)\boldsymbol{T}_y(u_4)\boldsymbol{R}_x(\theta_4)\boldsymbol{R}_y(\theta_5)\boldsymbol{R}_z(\theta_6)\boldsymbol{R}_z(\pi/2)\boldsymbol{T}_x(F)\boldsymbol{R}_z(\pi/2)\boldsymbol{T}_x(G)\\
&\boldsymbol{R}_z(-\pi/2)\boldsymbol{T}_x(N)\boldsymbol{R}_z(\pi/2)\boldsymbol{T}_x(O)\boldsymbol{T}_x(d_{11})\boldsymbol{R}_y(\alpha_{11})\boldsymbol{R}_z(\alpha_{12})
\end{aligned} \tag{15}$$

To characterize the FR, an open loop deviation vector for the door system is established, as illustrated in Figure 12. Subsequently, based on both the closed loop and open loop deviation vector models, and incorporating the variable specifications from Table 3, the closed loop and open loop assembly functions (Eq. (14) and Eq. (15)) are derived. Within this framework, the component Δz of the resultant vector $\boldsymbol{G}$ (obtained from the open-loop assembly function) along the z-axis explicitly represents the target FR.

3. Solution of vector loop model based on improved SOTA method

The SOTA method is a specialized tolerance analysis technique tailored for VL model. It primarily comprises the method of system moment (MSM), finite difference approximation for first- and second-order partial derivatives, non-linear system solving algorithm, and generalized lambda distribution (GLD) fitting. Based on the established assembly functions, the perturbation method alongside non-

linear system solver is utilized to evaluate the first- and second-order partial derivatives of the assembly variables with respect to the manufacturing variables. By incorporating the first four central moments of the manufacturing inputs, the corresponding first four moments of the assembly variables are analytically derived via the MSM. Subsequently, GLD fitting is employed to characterize the statistical distribution profiles of these assembly variables. Building upon this theoretical foundation, the improved SOTA method is formulated by introducing the ModFFD to enhance the computational efficiency of derivative evaluations, and by adopting Singular Value Decomposition (SVD) to robustly resolve the underdetermined assembly equations

3.1 Method of system moment

The MSM is a mathematical approach that evaluates the system output by utilizing the mapping relationship between the system's input and output variables, alongside the statistical distribution information of the inputs. It estimates the first four moments of the system output y_i based on the expected values and the first four moments of the input random variables x_j (j = 1, 2, …, n). The comprehensive theoretical expansions are detailed in Ref. [18].

In the context of the 3D VL model, the input variables x_j correspond to the component links, specifically representing manufacturing variables such as dimensional and geometric feature deviations. Conversely, the output variables y_i correspond to the closing links, representing assembly variables such as adaptive assembly adjustments or target FR. The nonlinear mapping relationship between the inputs and outputs is strictly governed by the assembly functions. In practice, by utilizing theoretical distributional assumptions or empirical data fitting to ascertain the distributions and statistical parameters of the input variables x_j, the first four moments of the output y_i can be subsequently derived.

3.2 Modified forward finite difference method

Obtaining the first four moments of the system output necessitates the evaluation of the first- and second-order partial derivatives of the output variables with respect to the input variables. However, traditional algorithms incur prohibitively immense computational costs when dealing with a large number of variables and high derivative orders. To overcome this computational bottleneck, the ModFFD is introduced. This approach significantly reduces the number of required system response evaluations while strictly preserving algorithmic accuracy, thereby drastically enhancing the computational efficiency of derivative estimations [19]. This method computes the unknown higher-order partial derivatives of the system by solving the following system of linear equations.

$$\boldsymbol{A}\boldsymbol{g} = \boldsymbol{d} \tag{16}$$

Where $\boldsymbol{A}$ denotes the coefficient matrix associated with the partial derivatives, $\boldsymbol{g}$ is the vector comprising the unknown higher-order partial derivatives, and $\boldsymbol{d}$ represents the system responses under various perturbation values of the input variables, which can be obtained through numerical simulations.

3.3 Newton-Raphson iterative method

In the 3D VL model, the implicit assembly functions exhibit highly non-linear characteristics, necessitating the application of non-linear numerical solving methods. Given that the Newton-Raphson iterative method possesses superior convergence speed in solving non-linear systems, it is utilized to solve the closed-loop assembly equations (the response vector $\boldsymbol{d}$ required in the aforementioned procedure is evaluated via this method). Reference [8] details the procedure of applying this method to solve closed-loop assembly equations. however, its application is strictly limited to determined systems. In the 3D VL model analysis of complex assemblies, when assembly clearances are taken into account, the number of unknown assembly variables frequently exceeds the number of available equations. This inevitably transforms the system into an underdetermined state, thereby demanding specialized solution strategies.

When the system is determined, the standard Newton-Raphson iterative equation can be written as:

$$\boldsymbol{E}\Delta\boldsymbol{y}_0 = \boldsymbol{F} \tag{17}$$

Where matrices $\boldsymbol{E}$ and $\boldsymbol{F}$ denote the iteration parameter matrices, respectively, and $\Delta\boldsymbol{y}_0$ represents the infinitesimal increment of the assembly variables.

When the system is either underdetermined or overdetermined, the problem can be reformulated into a least-squares problem. To enhance numerical stability and accommodate a broader range of scenarios, SVD is employed for the solution. By applying SVD to $\boldsymbol{E}$, the optimal numerical solution for Eq. (17) is given by:

$$\Delta\boldsymbol{y}_0 = \boldsymbol{V}\boldsymbol{\Sigma}^{+}\boldsymbol{U}^{\mathrm{T}}\boldsymbol{F} \tag{18}$$

Where $\boldsymbol{U}$ is a 6 × 6 orthogonal matrix, $\boldsymbol{\Sigma}$ is a $6\times n$ diagonal matrix (with singular values on the diagonal), and $\boldsymbol{V}$ is an $n \times n$ orthogonal matrix, $\boldsymbol{\Sigma}^{+}$ denotes the pseudo-inverse of $\boldsymbol{\Sigma}$. Subsequently, substituting the $\Delta\boldsymbol{y}_0$ obtained via this method into the Newton-Raphson method for iteration yields the least-squares solution that satisfies the precision requirements.

For the open loop assembly function (Eq. (2)), it is typically necessary to iteratively solve the closed loop assembly function first. Once the assembly variables required for the open-loop assembly function are determined, they are directly substituted into the open-loop assembly function to calculate the FR.

3.4 Generalized lambda distribution fitting

After obtaining the first four moments of the assembly variable y_i via the aforementioned steps, it is necessary to fit its distribution to evaluate whether the assembly variable satisfies the design requirements. The GLD exhibits excellent adaptability to a wide variety of distribution curves, and its parameter estimation relies solely on the first four moments of the sample data [20], which is highly compatible with the MSM. Therefore, the GLD is employed in the SOTA method to conduct distribution fitting for the results.

3.5 Improved SOTA solution procedure

As illustrated in Figure 13, the solution procedure of the improved SOTA method for the VL model comprises the following steps:

(1) Based on information such as the assembly geometric structure, tolerance items, and analysis requirements, determine the FR, the assembly variables $\boldsymbol{y} = (y_1, y_2,\ldots, y_n)^{\mathrm{T}}$, and the manufacturing variables $\boldsymbol{x} = (x_1, x_2,\ldots, x_n)^{\mathrm{T}}$. Construct the 3D VL model and derive the assembly functions.

(2) Evaluate the first- and second-order partial derivatives of the assembly variable y_i with respect to the manufacturing variable x_i, wherein the response vector $\boldsymbol{d}$ is obtained via the Newton-Raphson iterative method.

(3) Substitute the first- and second-order partial derivatives of y_i with respect to x_i, along with the first four central moments of x_i, into MSM to obtain the first four moments of the assembly variable y_i.

(4) Based on the first four moments of y_i, utilize the GLD to perform distribution fitting, generate its distribution plot, and conduct subsequent analyses.

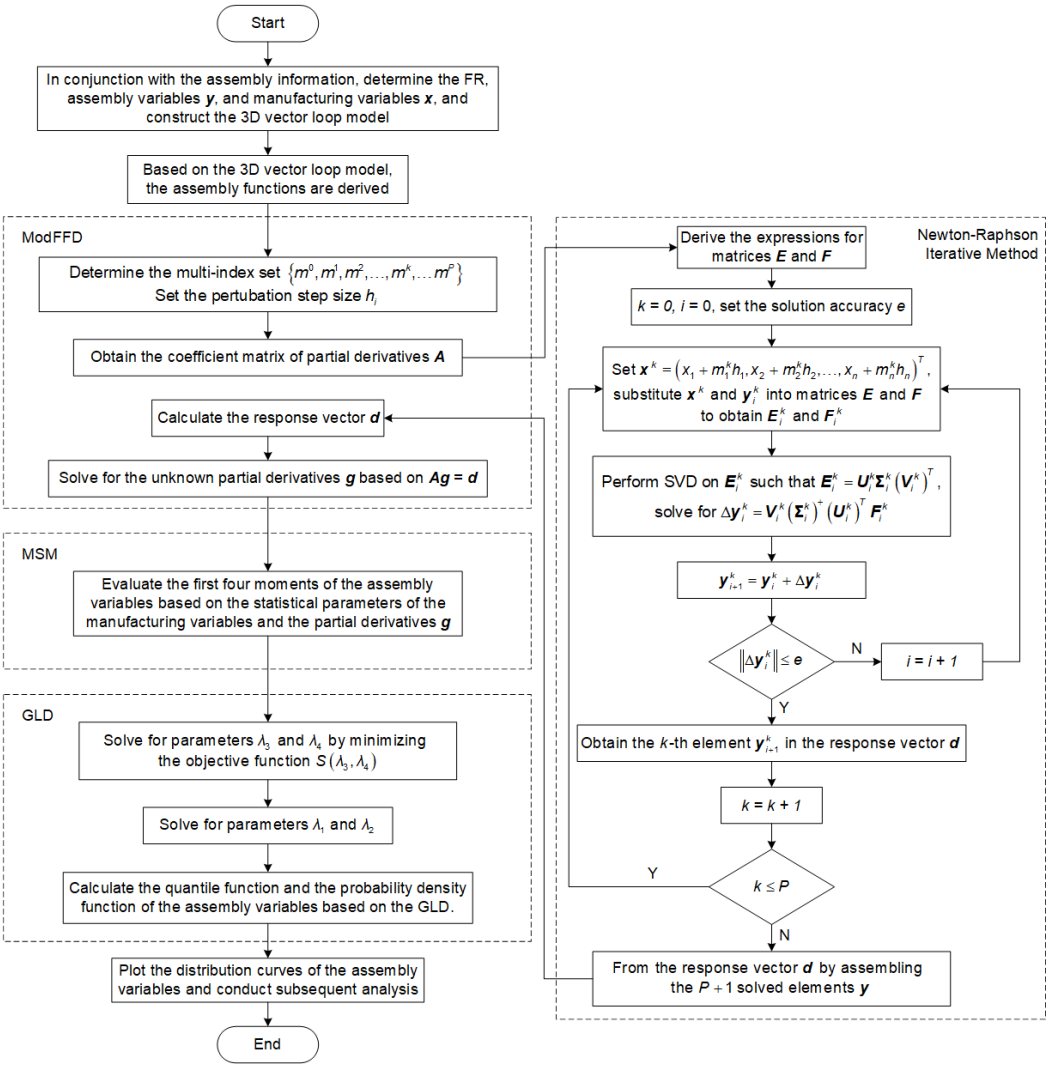


Figure 13 – Flowchart of the improved SOTA method.

4. Results and Discussion

Based on the improved SOTA method presented in Section 3.5, the VL model of the four-bar linkage bay door is solved. The simulation computing environment is as follows: CPU: 12th Gen Intel(R) Core(TM) i5-12490F 3.00 GHz; Programming Language: Python 3.12.6.

Assuming that all manufacturing variables follow a normal distribution within their ±3σ deviation ranges (with a rejection rate of 0.27%), the means and standard deviations of the variables can be calculated by the following equations:

$$\mu_v = \frac{T_U - T_L}{3} \tag{19}$$

$$\sigma_v = \frac{T_U - \mu}{3} \text{ or } \frac{\mu - T_L}{3} \tag{20}$$

where μ_v and σ_v represent the mean and standard deviation of the variables, respectively; T_U and T_L denote the upper and lower tolerance limits of the variables, respectively. Based on the properties of the normal distribution, the first four central moments of the manufacturing variables can be derived. Furthermore, for equivalent manufacturing variables such as d_1, d_2, α_1 and α_2 derived from parallel structure deviations, the actual variables participating in the calculation should be the branch

deviation variables of the parallel structures, as specified by the corresponding expressions in Table 3.

The accuracy of the ModFFD is highly dependent on the selection of the step size h_i. Satisfactory results are generally obtained in most cases when the normalized step size is $\Delta x_i / \mu_{xi} \approx 0.01$ [21]. In tolerance analysis, however, the order of magnitude for part tolerances typically ranges from 1 mm to 10^{-3} mm. Therefore, when the order of magnitude of the tolerance is 10^{-2} or higher, 0.01 is directly adopted as the step size. Conversely, when the order of magnitude is below 10^{-2}, the standard deviation of the variables (derived from Eq. (20)) is utilized as the step size. This approach not only ensures compliance with the allowable tolerance limits but also aligns with the statistical distribution characteristics of the variables. The convergence precision for the Newton-Raphson iteration is set to 10^{-6} mm. This value is significantly smaller than the common order of magnitude for mechanical manufacturing tolerances, ensuring that numerical errors remain negligible compared to actual manufacturing deviations. Furthermore, owing to the quadratic convergence property of this iterative method, the specified precision is typically achieved within a few iterations, thereby avoiding the waste of computational resources.

Subsequently, the MSM is employed to evaluate the first four moments of the assembly variables. Furthermore, these obtained results are substituted into Eq. (15), and the identical procedure is applied to solve for the open-loop variable $\boldsymbol{G}$. During this process, the assembly variables in Eq. (14) are treated as the manufacturing variables affecting $\boldsymbol{G}$. Ultimately, the first four moments of Δz, representing the z-axis component of $\boldsymbol{G}$, are determined.

For comparative analysis, the results of the bay door vector loop model were obtained using the MCM, the NTM, and the original SOTA method, respectively. Additionally, the results of the bay door J-T model were evaluated using the MCM. These comparative results are summarized in Table 4, the first four moments of Δz were converted into four statistical parameters: mean, standard deviation, skewness coefficient, and kurtosis coefficient.

Table 4 – Statistical parameters of Δz.

Variable	Model	Solution method	Mean	Standard deviation	Skewness	Kurtosis
Δz	VL	MCM (N = 20000)	4.7021×10^{-3}	1.6806	-0.0022	3.0461
	VL	NTM (N = 20000)	4.4629×10^{-4}	1.6672	-0.0071	2.9688
	VL	original SOTA	7.7032×10^{-5}	1.6023	-0.1712	2.8886
	VL	improved SOTA	9.3264×10^{-5}	1.6224	0.0208	2.9803
	J-T	MCM (N = 20000)	7.733×10^{-4}	0.4302	-0.0424	2.9719

In tolerance analysis, the mean reflects the expected value or central tendency of the FR. Since all deviations in the bay door analysis are symmetrically distributed, the ideal mean of the FR should be zero. The standard deviation indicates the degree of dispersion in the FR deviation, characterizing its distribution under various σ requirements of the constituent links. When utilizing the VL model, the standard deviation calculated by the improved SOTA method is 1.6224 mm. This signifies that under the current tolerance design, there is a 99.73% probability that the step gap between the fuselage and the follow-up door falls within the interval of [-4.8672, 4.8672] mm. This range is then evaluated against the performance specifications to conduct a preliminary assessment of the accumulated assembly deviations. Compared to the standard deviations obtained from the MCM (N = 20000), the NTM (N = 20000), and the original SOTA method, the relative errors of the improved SOTA method are approximately 3.46%, 2.68%, and 1.25%, respectively, thereby verifying its accuracy. Furthermore, the skewness and kurtosis coefficients reflect the asymmetry of the distribution and its discrepancy from a normal distribution at the peaks and tails, respectively, aiding in revealing the general statistical characteristics of the FR. Because the SOTA method involves approximations and

truncations during the solution procedure, its results inevitably exhibit slight deviations from an ideal normal distribution.

Applying the statistical method based on the J-T model to conduct the 3D tolerance analysis of the four-bar linkage bay door yields a standard deviation of 0.4302, which presents a significant discrepancy compared to the result obtained by the improved SOTA method. This discrepancy arises because the J-T model fails to account for the rotational deviations around the axis and the overall kinematic constraints of the mechanism, for cylindrical features, the rotational deviation around the axis is defined as an invariant (exerting no influence on the tolerance analysis results). In actual closed-loop mechanisms, however, assembly adjustments introduce this deviation, which subsequently exerts a profound impact on the pose of the parts due to the leverage effect. Consequently, it is evident that the VL model is more representative of actual physical conditions when conducting tolerance analysis for complex kinematic mechanisms.

Table 5 – Computational efficiency of different solution methods.

Solution method	Theoretical computational load	time (s)
MCM (N = 20000)	N × average Newton-Raphson iterations	9936.5
NTM (N = 20000)		11144.1
original SOTA	($2n^2 + 1$) × average Newton-Raphson iterations	592.5
improved SOTA	($n^2 + 3n + 2$) / 2 × average Newton-Raphson iterations	217.8

As presented in Table 5, the total computational time of the SOTA method is substantially reduced compared to the MCM and the NTM. Furthermore, the improved SOTA method achieves an additional 63.2% reduction in computation time compared to the original SOTA method. The computational efficiency of the VL model primarily depends on the average number of Newton-Raphson iterations required to solve the closed-loop vector equations. This dependency manifests as the number of random samples in the MCM and the NTM, and as the number of evaluations for the first- and second-order partial derivatives in the SOTA method. The original and improved SOTA methods employ the traditional finite difference formulation and the ModFFD method, respectively, to evaluate these partial derivatives. Given n constituent links, the original SOTA method requires ($2n^2 + 1$) evaluations, whereas the improved SOTA method requires only ($n^2 + 3n + 2$) / 2 evaluations. In practical tolerance analysis, the number of constituent links is significantly smaller than the number of random samples required to achieve high-precision results; therefore, the SOTA method exhibits a pronounced efficiency advantage over statistical methods. For the bay door model, the number of constituent links in the closed-loop vector equations is n = 21. Consequently, the theoretical computational load is 883 × average Newton-Raphson iterations for the original SOTA method, and 253 × average Newton-Raphson iterations for the improved SOTA method. This represents a theoretical reduction in computational load of approximately 71.3%, which aligns closely with the 63.2% efficiency improvement observed in the actual simulation. This strong correlation demonstrates that the enhanced efficiency of the improved SOTA method is primarily attributable to the optimization achieved by the ModFFD method during the partial derivative evaluation phase.

Based on the solution obtained from the improved SOTA method, coupled with GLD fitting, the distribution plot of the FR Δz is generated, as illustrated in Figure 14. Specifically, the histogram represents the results of the MCM (N = 20000), while the curve denotes the GLD fitting results. The two exhibit a high degree of agreement, providing an intuitive visual representation of the assembly deviation distribution for the FR under the current tolerance design.

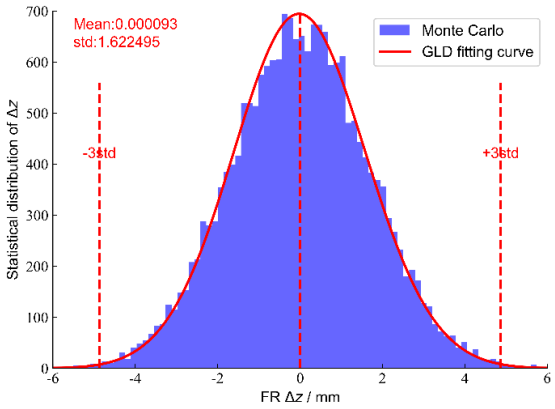


Figure 14 – Fitted distribution plot of Δ*z* based on the improved SOTA method.

5. Conclusions and Perspectives

(1) A simplified 3D tolerance modeling method, based on the SDT theory and the 3D vector loop model, is proposed for complex spatial mechanisms with multiple parallel structures. This method utilizes the SDT theory to provide an equivalent description of the deviations in parallel structures, thereby transforming the spatial mechanism into a planar mechanism. Furthermore, by taking relevant tolerance principles into account, it integrates feature mating deviations and geometric deviations into an equivalent comprehensive deviation. Subsequently, the 3D VL model is established according to the kinematic characteristics of the bay door and the specific analysis objectives. Under the tolerance design specified by HB5800-2021 and other relevant standards, the calculated standard deviation of the step gap between the follow-up door and the fuselage is 1.62 mm, which contrasts with the 0.43 mm result obtained using the J-T model. Because the proposed method accounts for the assembly adjustment deviations in the rotational direction around the axis as well as the overall kinematic constraints of the mechanism, it is more representative of actual physical conditions in the tolerance analysis of complex mechanisms. Consequently, it effectively addresses the assembly deviation modeling challenges for multi-parallel spatial mechanisms, as exemplified by the aircraft four-bar linkage bay door.

(2) Targeting the simplified 3D tolerance modeling method for complex mechanisms with multiple parallel structures, a more efficient and robust improved solution procedure is developed based on the SOTA method. By incorporating the ModFFD method into the SOTA framework, the computational cost associated with evaluating the first- and second-order partial derivatives is effectively reduced. Furthermore, utilizing SVD to solve the least-squares problem significantly enhances the numerical stability of the solution and successfully addresses the challenge of solving underdetermined assembly constraint equations. Compared to the MCM, the NTM, and the original SOTA method, the relative errors of the standard deviation for the FR of the four-bar linkage bay door obtained by the proposed method are approximately 3.46%, 2.68%, and 1.25%, respectively. Additionally, the computational time is reduced by 63.2% compared to the original SOTA method. While maintaining the requisite accuracy of the tolerance analysis, this approach significantly improves both computational efficiency and generality, paving the way for future research on nonlinear tolerance analysis under applied loads.

(3) Integrating the proposed simplified 3D tolerance model with the improved SOTA solution method enables the effective implementation of 3D tolerance analysis for complex mechanism products featuring multiple parallel structures, as exemplified by the aircraft four-bar linkage bay door. This approach successfully addresses the challenge of predicting the accumulation of assembly deviations induced by multi-parallel structures, thereby providing a robust methodological framework and workflow reference for the 3D tolerance analysis of similar complex mechanisms.

For future work, building upon the proposed 3D tolerance analysis method, we will further integrate finite element analysis of complex mechanisms to investigate the underlying effects of applied loads on assembly deviations under actual service conditions. The ultimate objective is to develop advanced techniques and methodologies for nonlinear 3D tolerance analysis.

6. Contact Author Email Address

mailto: yangrui@dlut.edu.cn

7. Copyright Statement

The authors confirm that they, and/or their company or organization, hold copyright on all of the original material included in this paper. The authors also confirm that they have obtained permission, from the copyright holder of any third party material included in this paper, to publish it as part of their paper. The authors confirm that they give permission, or have obtained permission from the copyright holder of this paper, for the publication and distribution of this paper as part of the ICAS proceedings or as individual off-prints from the proceedings.

References

[1] Li JY, Zhao G, Zhang PF, et al. A digital twin-based on-site quality assessment method for aero-engine assembly. *Journal of Manufacturing Systems*, Vol. 71, pp 565-580, 2023.

[2] Zhang H, Li Y, Xue D, et al. Digital twin technology facilitates precision improvement in complex product assembly: a progressive deduction method of data-driven tolerance allocation. *Advanced Engineering Informatics*, Vol. 62, pp 102790, 2024.

[3] Yu J, Zhao Y, Wang H et al. Tolerance analysis of mechanical assemblies based on the product of exponentials formula. *Proceedings of the Institution of Mechanical Engineers, Part B: Journal of Engineering Manufacture*, Vol. 232, No. 14, pp 2616-2626, 2018.

[4] Liu S, Yu HD, Xia ZK et al. A new virtual functional element method for deviation prediction of assembled structures with parallel connection chain. *CIRP Journal of Manufacturing Science and Technology*, Vol. 48, pp 42-54, 2024.

[5] Cao YL, Liu T and Yang JX. A comprehensive review of tolerance analysis models. *The International Journal of Advanced Manufacturing Technology*, Vol. 97, No. 5, pp 3055-3085, 2018.

[6] Chen H, Jin S, Li ZM et al. A comprehensive study of three dimensional tolerance analysis methods. *Computer-Aided Design*, Vol. 53, pp 1-13, 2014.

[7] Glancy CG and Chase KW. A second-order method for assembly tolerance analysis. *25th Design Automation Conference*, Las Vegas, Nevada, USA, pp 977-984, 1999.

[8] Cao YL, Liu T, Yang JX et al. A novel tolerance analysis method for three-dimensional assembly. *Proceedings of the Institution of Mechanical Engineers, Part B: Journal of Engineering Manufacture*, Vol. 233, No. 7, pp 1818-1827, 2019.

[9] Zhao DP, Wang GF, Hui JZ et al. A precision analysis method for the kinematic assembly of complex products based on equivalence of deviation source. *Assembly Automation*, Vol. 40, No. 3, pp 447-460, 2020..

[10] Corrado A and Polini W. Tolerance analysis tools for fixture design: a comparison. *Procedia CIRP*, Vol. 92, pp 112-117, 2020.

[11] Kosec P, Skec S and Miler D. A comparison of the tolerance analysis methods in the open-loop assembly. *Advances in Production Engineering & Management*, Vol. 15, No. 1, pp 44-56, 2020.

[12] Schaechtl P, Hallmann M, Schleich B. Tolerance analysis of additively manufactured non-assembly mechanisms considering joint clearance. *Procedia CIRP*, Vol. 92, pp 27-32, 2020.

[13] Maltauro M, Meneghello R and Concheri G. A second-order tolerance analysis approach to statistical virtual assembly for rigid parts. *The International Journal of Advanced Manufacturing Technology*, Vol. 131, No. 1, pp 437-446, 2024.

[14] Li JY, Zhao G, Wei JH, et al. Assembly simulation and optimization method for underconstrained frame structures of aerospace vehicles. *Aerospace*, Vol. 11, No. 8, pp 689, 2024.

[15] Zhao DP, Yuan Z, Zhao XS et al. An assembly accuracy analysis method for weak rigid components. *Machines*, Vol. 13, No. 8, pp 694, 2025.

[16] Hallmann M, Schleich B and Wartzack S. How to consider over-constrained assemblies with gaps in tolerance-cost optimization? *Procedia CIRP*, Vol. 92, pp 88-93, 2020.

[17] Wu YG. The correlational design method of the dimension tolerance and geometric tolerance for applying material conditions. *The International Journal of Advanced Manufacturing Technology*, Vol. 97, No. 5, pp 1697-1710, 2018.

[18] Cox ND. Tolerance analysis by computer. *Journal of Quality Technology*, Vol. 11, No. 2, pp 80-87, 1979.

[19] Paudel A, Gupta S, Thapa M, et al. Higher-order Taylor series expansion for uncertainty quantification with efficient local sensitivity. *Aerospace Science and Technology*, Vol. 126, pp 107574, 2022.

[20] Karian ZA and Dudewicz EJ. Comparison of GLD fitting methods: superiority of percentile fits to moments in L^2 norm. *Journal of the Iranian Statistical Society*, Vol. 2, No. 2, pp 171-187, 2022.

[21] Thapa M, Mulani SB and Walters RW. A new non-intrusive polynomial chaos using higher order sensitivities. *Computer Methods in Applied Mechanics and Engineering*, Vol. 328, pp 594-611, 2018.